Networked Decentralized Control of Adaptive Structures

Alexander Warsewa, Julia L. Wagner, Michael Böhm, Oliver Sawodny, and Cristina Tarín
Institute for System Dynamics, University of Stuttgart, 70563 Stuttgart, Germany
Email: warsewa@isys.uni-stuttgart.de

Abstract—Adaptive structures, i.e. structures equipped with active load-bearing elements, enable ultra-lightweight construction but also come with additional challenges. Control of such structures needs to be performed in real-time with high reliability and robustness. Decentralization provides a means to reduce cost and increase both redundancy and reliability. In this contribution, we introduce a method for decentralized state estimation and control of adaptive high-rise structures. Subsystem models are derived from a global Finite Element (FE) model of the structure using model order reduction techniques which enables the use of distributed and Decentralized Information Filters (DDIF) for local observers. By projecting between local state spaces, networked control of decentralized units can be realized. We compare decentralized controllers with different levels of interconnectedness to centralized Linear Quadratic Gaussian (LQG) control of the same structure and conclude that similar or even better performance can be achieved, depending on the requirements on energy consumption and damping response.

Index Terms—Decentralized control, adaptive structures, networked control, fourth term, sensor fusion, structural dynamics

I. Introduction

A growing trend towards urbanization and global population growth combined with decreasing resources lead to ever increasing problems in the construction sector. Not only is it the field already responsible for a major amount of global energy consumption, construction and operation of buildings also produces a considerable amount of greenhouse gas [1], [2]. The introduction of *adaptive structures* enables *ultra-lightweight* constructions by means of active load-bearing elements integrated into the structure that are used to compensate loads such as strong winds. Not having to passively withstand extreme loads, the structures can be realized using considerably less raw materials and associated energy [3]. However, the control of an adaptive structure is not a trivial task and requires suitable methods for safe and reliable operation. We focus on the real-time state estimation and control of high-rise structures here. Information on the structural deformation and internal load distribution is only available from a limited number of sensors in practice. Model based sensor fusion techniques are commonly employed in such a case to estimate the full state of the structure, which is required by a controller to efficiently damp structural vibrations. Even though the concept of adaptive structures is relatively new, structural control has been a field of research for a longer time. See [4], [5] for surveys on the topic.

In case estimation and control are conducted on a central unit, communication of a relatively large amount of sensor data over long distances is required. Additionally, failure of the central control unit is to be avoided at all cost. Decentralization alleviates some of those issues but is not easily realized for structures with strong physical coupling between states. Regarding the decentralized control of complex or large-scale systems in general, see e.g. [4] and [6]. With respect to tall buildings, only a limited number of publications is available on their decentralized control. In most of them, local subsystems are derived by directly partitioning the structure's FE model into substructures [7]-[10]. Coupling between the structures is then either neglected as in [9] or included by modeling interconnection effects at the substructure interfaces. The former leads to inferior performance compared to a centralized control and the latter requires online estimation of coupling forces which is sensitive to disturbances. Lynch and Law [10] propose to only partition the input and output matrices while retaining the global dynamic model. However, they do not consider state estimation which would perform poorly when using only local sensor information to estimate the global state. Instead of partitioning the FE model, we employ model order reduction techniques to derive subsystem dynamics in local degrees of freedom (DOFs) as previously shown in [11]. This increases local accuracy while retaining the global dynamics in good approximation. By projecting between the local state spaces using transformations, communication between control units can be realized in a straightforward fashion. We use the *distributed and decentralized information filter* (DDIF), as introduced by Mutambara [12], for real-time state estimation and consider different levels of interconnectedness between modules. Ideal communication between modules is assumed here and a linear quadratic regulator (LQR) is used for damping the vibrations in each actuated subsystem. Our approach can be used to design decentralized controllers with performance comparable to centralized control. Thus, the benefits of decentralization, i.e. redundancy and cost-effectiveness, are obtained without sacrificing efficiency.

Manuscript received December 7, 2019, revised April 25, 2020
The authors acknowledge the funding of this work by the German Research Foundation (DFG – Deutsche Forschungsgemeinschaft) as part of the Collaborative Research Center 1244 (SFB) "Adaptive Skins and Structures for the Built Environment of Tomorrow" / projects B02, B04.
Corresponding author email: warsewa@isys.uni-stuttgart.de.
doi:10.12720/jcm.15.6.496-502

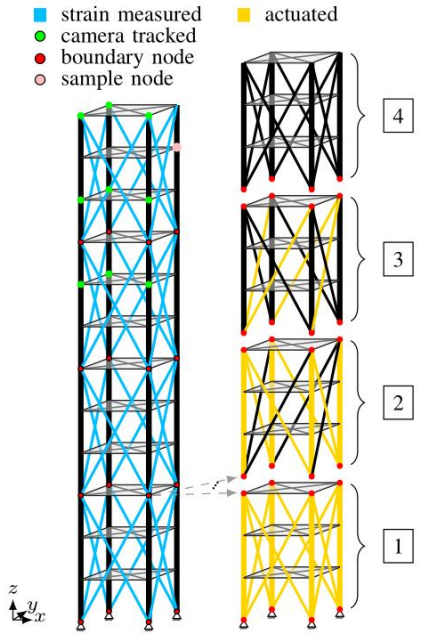

Fig. 1. Schematic drawing of the adaptive structures demonstrator building and its decomposition into four modules which are to be controlled in a decentralized fashion.

TABLE I: GEOMETRY AND MATERIAL PARAMETERS

Elements	Parameter	Symbol	Value	Unit
	Density	ρ	7850	kg/m^3
	Young's Modulus	E	210	GPa
	Poisson's ratio	ν	0.3	
Vertical columns, quadratic hollow profiles	Length	L_v	3	m
	Width	w_v	0.3	m
	Wall thickness	t_v	0.01	m
Horizontal links, rectangular hollow profiles	Length	L_h	4.75	m
	Width	w_h	0.504	m
	Height	h_h	0.12	m
	Wall thickness	t_h	0.008	m
Horizontal diagonal links	Length	L_{hd}	6.73	m
	Width	w_{hd}	0.01	m
	Height	h_{hd}	0.06	m
Diagonal links	Length	L_{vd}	10.18	m
	Width	w_{vd}	0.15	m
	Height	h_{vd}	0.012	m

II. SYSTEM DESCRIPTION

For testing the decentralized control concept introduced in this contribution, a simulation model of an adaptive structures demonstrator building to be constructed on campus of the University of Stuttgart is used. It is shown in Fig. 1 and is explained in more detail in Sec. II-A this is followed by a brief section on modal analysis which we employ to reduce the system order for simulation purposes.

A. Structure Model

As illustrated in Fig. 1, the demonstrator building consists of 12 stories with a quadratic floor layout. Floor plates are modeled with two intersecting horizontal diagonal links each. Vertical diagonal bracings are used to enhance the stiffness of the structure which subdivide the structure into the four symmetrical modules shown on the right hand side. Those modules are considered as local subsystems for decentralized control in the following. They are equipped with a varying number of hydraulic actuators connected in parallel to the respective truss elements as described in [13]. Actuator dynamics are assumed negligible such that their influence can be modeled as simple force inputs. All truss elements are composed of structural steel. The structural dynamics are obtained from a FE model using the parameters in Table I.

$$\boldsymbol{M}\ddot{\boldsymbol{q}}(t) + \boldsymbol{D}\dot{\boldsymbol{q}}(t) + \boldsymbol{K}\boldsymbol{q}(t) = \boldsymbol{F}_u\boldsymbol{u}(t), \quad t > 0 \qquad (1)$$
$$\boldsymbol{q}(t=0) = \boldsymbol{q}_0, \quad \dot{\boldsymbol{q}}(t=0) = \boldsymbol{q}_1.$$

with the ground nodes being fixed except for the rotations about the x- and y-axis, a total of $n = 296$ DOFs $\boldsymbol{q}(t)$ results. In (1), $\boldsymbol{M} \in \mathbb{R}^{n\times n}$ and $\boldsymbol{K} \in \mathbb{R}^{n\times n}$ are the mass and stiffness matrix and $\boldsymbol{F}_u \in \mathbb{R}^{n\times m}$ maps the actuator forces $\boldsymbol{u}(t)$ to the model's DOFs, where $m = 24$ is the number of actuators. Rayleigh damping is assumed such that the damping matrix $\boldsymbol{D}$ is obtained as a linear combination of $\boldsymbol{M}$ and $\boldsymbol{K}$

$$\boldsymbol{D} = \alpha_1\boldsymbol{M} + \alpha_2\boldsymbol{K}, \qquad (2)$$

with the damping coefficients $\alpha_1$and α_2.

Information on the structural deformation is obtained using two different measurement systems - an optical camera system and strain gauge sensors. The latter measure the length changes of the diagonal bracings which are highlighted in blue in Fig. 1. The optical measurement system tracks the in-plane displacements of the nodes marked with green dots with high accuracy using cameras located at a certain distance from the building. For a detailed description of the measurement principle, see [14]. Sensor fusion of both measurement systems is performed by the observers described in Sec IV-A.

B. Modal Analysis

Modal analysis is employed on various occasions throughout this article to obtain reduced order models by truncation of high-frequency system eigenmodes. We only give a brief summary of this common technique here. For a detailed discussion, see e.g. [15]. Using the ansatz

$$\boldsymbol{q}(t) = \varphi_i^{j\omega_i t}, \qquad (3)$$

where ω_i with $i \in 1 \ldots n$ are the structure's eigenvalues and φ_i the corresponding eigenvectors, the dynamic equations (1) without damping and input terms can be reformulated as

$$(\boldsymbol{K} - \omega_i^2\boldsymbol{M})\varphi_i = 0. \qquad (4)$$

One can solve this equation for ω_i and φ_i where the latter are not uniquely determined. They are selected such that $\boldsymbol{\Phi}^{\mathrm{T}}\boldsymbol{M}\boldsymbol{\Phi} = \mathbf{I}$ with $\boldsymbol{\Phi} = [\varphi_1 \quad \cdots \quad \varphi_n]^{\mathrm{T}}$. A lower order simulation model is then obtained by approximating $\boldsymbol{q}(t)$ with a reduced number of lowest magnitude primary eigenmodes $\boldsymbol{\eta}_{\mathrm{p}}(t) \in \mathbb{R}^{n_{\mathrm{p}}}$ such that $\boldsymbol{q}(t) \approx \boldsymbol{\Phi}_{\mathrm{p}}\boldsymbol{\eta}_{\mathrm{p}}(t)$. Left-multiplying (1) with the transpose of $\boldsymbol{\Phi}_{\mathrm{p}}$ yields

$$\ddot{\boldsymbol{\eta}}_{\mathrm{p}} + \boldsymbol{D}^{*}\dot{\boldsymbol{\eta}}_{\mathrm{p}}(t) + \boldsymbol{K}^{*}\boldsymbol{\eta}_{\mathrm{p}}(t) = \boldsymbol{F}_{u}^{*}\boldsymbol{u}(t), \quad t > 0, \tag{5}$$

where $\boldsymbol{D}^{*} = \boldsymbol{\Phi}_{\mathrm{p}}^{\mathrm{T}}\boldsymbol{D}\boldsymbol{\Phi}_{\mathrm{p}}$ is the modal damping matrix, $\boldsymbol{K}^{*}$a diagonal matrix of primary eigenvalues and $\boldsymbol{F}_{u}^{*} = \boldsymbol{\Phi}_{\mathrm{p}}^{\mathrm{T}}\boldsymbol{F}_{u}$. A state space representation of (5) is obtained by choosing the state vector as $\boldsymbol{x}(t) = [\boldsymbol{\eta}_{\mathrm{p}} \quad \dot{\boldsymbol{\eta}}_{\mathrm{p}}]^{\mathrm{T}}$

$$\begin{aligned} \dot{\boldsymbol{x}}(t) &= \begin{bmatrix} 0 & I \\ -\boldsymbol{K}^{*} & -\boldsymbol{D}^{*} \end{bmatrix}\boldsymbol{x}(t) + \begin{bmatrix} 0 \\ \boldsymbol{F}_{u}^{*} \end{bmatrix}\boldsymbol{u}(t), \\ \boldsymbol{y}(t) &= \boldsymbol{C}\boldsymbol{x}(t), \quad \boldsymbol{x}(t=0) = \boldsymbol{x}_{0}. \end{aligned} \tag{6}$$

The output matrix $\boldsymbol{C}$ relates the state $\boldsymbol{x}(t)$ to the system output $\boldsymbol{y}(t)$ which is composed of the quantities measured by camera system and strain gauges.

III. Reduced Order Local Models

Local models for decentralized estimation and control are obtained from the global dynamics (1) by means of model order reduction techniques. We apply a method that we previously employed in [11] to derive local subsystems for decentralized state estimation of a two-dimensional diagrid high-rise structure. Subsystem dynamics in terms local DOFs are obtained by applying a combination of Guyan condensation and SEREP to the global FE model. First of all, the global DOF vector $\boldsymbol{q}(t)$is divided into active DOFs $\boldsymbol{q}_{\mathrm{a}}(t) \in \mathbb{R}^{n_{\mathrm{a}}}$ (i. e. the local DOFs of a module) and dependent DOFs $\boldsymbol{q}_{\mathrm{d}}(t) \in \mathbb{R}^{n-n_{\mathrm{a}}}$ and rearranged such that

$$\boldsymbol{q}_{\mathrm{f}}(t) = [\boldsymbol{q}_{\mathrm{a}}(t) \quad \boldsymbol{q}_{\mathrm{d}}(t)]^{\mathrm{T}} = \boldsymbol{P}_{\pi}\boldsymbol{q}(t). \tag{7}$$

Here, $\boldsymbol{P}_{\pi}$ is the corresponding permutation matrix. It is used to rearrange both mass and stiffness matrix accordingly

$$\boldsymbol{K}_{\mathrm{f}} = \boldsymbol{P}_{\pi}\boldsymbol{K}\boldsymbol{P}_{\pi}^{\mathrm{T}} = \begin{bmatrix} \boldsymbol{K}_{\mathrm{aa}} & \boldsymbol{K}_{\mathrm{ad}} \\ \boldsymbol{K}_{\mathrm{da}} & \boldsymbol{K}_{\mathrm{dd}} \end{bmatrix}, \quad \boldsymbol{M}_{\mathrm{f}} = \boldsymbol{P}_{\pi}\boldsymbol{M}\boldsymbol{P}_{\pi}^{\mathrm{T}}. \tag{8}$$

Guyan condensation, as introduced in [16], then proceeds by eliminating the dependent DOFs $\boldsymbol{q}_{\mathrm{d}}(t)$ by means of a transformation, approximating $\boldsymbol{q}_{\mathrm{f}}(t)$ as

$$\boldsymbol{q}_{\mathrm{f}}(t) \approx \begin{bmatrix} I \\ -\boldsymbol{K}_{\mathrm{dd}}^{-1}\boldsymbol{K}_{\mathrm{da}} \end{bmatrix}\boldsymbol{q}_{\mathrm{a}}(t) = \boldsymbol{T}_{\mathrm{G}}\boldsymbol{q}_{\mathrm{a}}(t), \tag{9}$$

where $\boldsymbol{\Phi}_{\mathrm{a}} \in \mathbb{R}^{n_{\mathrm{a}} \times n_{\mathrm{f}}}$ is the Guyan transformation. Guyan condensation is a static condensation technique and, as such, does not preserve the dynamic behavior of the system accurately. This disadvantage can be compensated by combining it with the SEREP transformation which retains the dynamics of a reduced number of system eigenmodes $\boldsymbol{\eta}_{\mathrm{r}}(t)$ in the local model. The corresponding eigenvectors $\boldsymbol{\Phi}_{\mathrm{r}} \in \mathbb{R}^{n_{d} \times n_{r}}$ are rearranged using $\boldsymbol{P}_{\pi}$ such that

$$\boldsymbol{q}_{\mathrm{f}}(t) \approx \boldsymbol{P}_{\pi}\boldsymbol{\Phi}_{\mathrm{r}}\boldsymbol{\eta}_{\mathrm{r}}(t) = \begin{bmatrix} \boldsymbol{\Phi}_{\mathrm{a}} \\ \boldsymbol{\Phi}_{\mathrm{d}} \end{bmatrix}\boldsymbol{\eta}_{\mathrm{r}}, \tag{10}$$

where $\boldsymbol{\Phi}_{\mathrm{a}} \in \mathbb{R}^{n_{\mathrm{a}} \times n_{\mathrm{r}}}$ maps $\boldsymbol{\eta}_{\mathrm{r}}(t)$ to the active DOFs and $\boldsymbol{\Phi}_{\mathrm{d}} \in \mathbb{R}^{n_{\mathrm{d}} \times n_{\mathrm{r}}}$ to the dependent ones. According to [17], SEREP transformation then relates $\boldsymbol{q}_{\mathrm{a}}(t)$ to the rearranged global DOF vector by means of the generalized inverse $\boldsymbol{\Phi}_{\mathrm{a}}^{+} = (\boldsymbol{\Phi}_{\mathrm{a}}^{\mathrm{T}}\boldsymbol{\Phi}_{\mathrm{a}})^{-1}\boldsymbol{\Phi}_{\mathrm{a}}^{\mathrm{T}}$ as follows

$$\boldsymbol{q}_{\mathrm{f}}(t) \approx \boldsymbol{P}_{\pi}\boldsymbol{\Phi}_{\mathrm{r}}\boldsymbol{\Phi}_{\mathrm{a}}^{+}\boldsymbol{q}_{\mathrm{a}}(t) = \boldsymbol{T}_{\mathrm{U}}\boldsymbol{q}_{\mathrm{a}}(t)\,. \tag{11}$$

Here, $\boldsymbol{T}_{\mathrm{U}}$ is the SEREP transform. Since it retains the same set of active DOFs $\boldsymbol{q}_{\mathrm{a}}(t)$ as $\boldsymbol{T}_{\mathrm{G}}$, a hybrid transformation can be constructed, as stated e. g. in [18]

$$\boldsymbol{T}_{\mathrm{H}} = \boldsymbol{T}_{\mathrm{G}} + (\boldsymbol{T}_{\mathrm{G}} - \boldsymbol{T}_{\mathrm{U}})[\boldsymbol{\Phi}_{\mathrm{a}}\boldsymbol{\Phi}_{\mathrm{a}}^{\mathrm{T}}\boldsymbol{M}_{\mathrm{f}}\boldsymbol{T}_{\mathrm{U}}]. \tag{12}$$

The SEREP-Guyan transformation $\boldsymbol{T}_{\mathrm{H}}$ combines the advantages of both transformations and is numerically stable. Left-multiplying (1) with the transpose of $\boldsymbol{T}_{\mathrm{H}}$, the local dynamics in the active DOFs $\boldsymbol{q}_{i}(t)$ of module i, with $i \in \{1,2,3,4\}$ are obtained as

$$\boldsymbol{M}_{i}\ddot{\boldsymbol{q}}_{i}(t) + \boldsymbol{D}_{i}\dot{\boldsymbol{q}}_{i}(t) + \boldsymbol{K}_{i}\boldsymbol{q}_{i}(t) = \boldsymbol{F}_{ui}\boldsymbol{u}_{i}(t), t > 0. \tag{13}$$

Depending on the size of local subsystems, the number of DOFs can still be prohibitive for real-time estimation and control on low-cost hardware. To further reduce computational effort, modal analysis is employed to reduce the order of the local systems to the dynamics of a reduced number of local eigenmodes $\boldsymbol{\eta}_{i}(t) \in \mathbb{R}^{n_{i}}$ such that

$$\boldsymbol{q}_{i}(t) \approx \boldsymbol{\Phi}_{i}\boldsymbol{\eta}_{i}(t). \tag{14}$$

As above, choosing the local state vector as $\boldsymbol{x}_{i}(t) = [\boldsymbol{\eta}_{i}(t) \quad \dot{\boldsymbol{\eta}}_{i}(t)]^{\mathrm{T}}$ leads to the state space formulation

$$\dot{\boldsymbol{x}}_{i}(t) = \underbrace{\begin{bmatrix} \boldsymbol{0} & I \\ -\boldsymbol{K}_{i}^{*} & -\boldsymbol{D}_{i}^{*} \end{bmatrix}}_{\boldsymbol{A}_{i}}\boldsymbol{x}_{i}(t) + \underbrace{\begin{bmatrix} 0 \\ \boldsymbol{F}_{ui}^{*} \end{bmatrix}}_{\boldsymbol{B}_{i}}\boldsymbol{u}_{i}(t), \tag{15}$$

$$\boldsymbol{y}_{i}(t) = \boldsymbol{C}_{i}\boldsymbol{x}_{i}(t), \quad \boldsymbol{x}_{i}(t=0) = \boldsymbol{x}_{i0}.$$

The local output matrix $\boldsymbol{C}_{i}$ relates the local state vector to the measured quantities, i.e. deformations tracked by the camera system and strain measurements.

IV. State Estimaton and Control

In the following, the local subsystems introduced in the previous section are used for decentralized observer and controller design. Local estimators are realized as DDIF according to [12] in Sec. IV-A. For the decentralized controllers, LQR control is performed on the local subsystems which is presented in Sec. IV-B.

A. Decentralized and Distributed Observers

With the DDIF, estimation is carried out in discrete time. Therefore, the dynamics (15) of each module are transformed according to [19]

$$\boldsymbol{F}_{i} = e^{\boldsymbol{A}_{i}\Delta t}, \quad \boldsymbol{G}_{i} = (\boldsymbol{F}_{i} - I)\boldsymbol{A}_{i}^{-1}\boldsymbol{B}_{i}, \tag{16}$$

where $\boldsymbol{F}_{i} \in \mathbb{R}^{n_{i} \times n_{i}}$ and $\boldsymbol{G}_{i} \in \mathbb{R}^{n_{i} \times m_{i}}$ are the discrete time state transition and input matrix respectively. As stated above, the local dynamics are obtained by distribution of the global model. Using the transformations of Sec. III, the local state vector can be expressed in terms of the global state

$$\boldsymbol{x}_{i}[k] = \begin{bmatrix} \boldsymbol{\Phi}_{i}^{\mathrm{T}}\boldsymbol{T}_{\mathrm{H}i}^{\mathrm{T}}\boldsymbol{P}_{\pi i} & 0 \\ 0 & \boldsymbol{\Phi}_{i}^{\mathrm{T}}\boldsymbol{T}_{\mathrm{H}i}^{\mathrm{T}}\boldsymbol{P}_{\pi i} \end{bmatrix}\boldsymbol{x}_{\mathbf{i}}[k] = \boldsymbol{T}_{i}\boldsymbol{x}[k], \tag{17}$$

where $\boldsymbol{x_i}[k] = [\boldsymbol{q_i}[k] \quad \dot{\boldsymbol{q}}_i[k]]^{\mathrm{T}}$.The information filter is essentially an algebraic transformation of the Kalman filter that is more convenient for decentralization. Estimation is carried out in *information space* rather than in state space where the *information state vector* $\hat{\boldsymbol{y}}_i[k]$ is related to the state estimate $\hat{\boldsymbol{x}}_i[k]$ as follows

$$\hat{\boldsymbol{y}}_i[k] = (\boldsymbol{P}_i[k])^{-1}\hat{\boldsymbol{x}}_i[k] = \boldsymbol{Y}_i[k]\hat{\boldsymbol{x}}_i[k]. \quad (18)$$

The *information matrix* $\boldsymbol{Y}_i[k] \in \mathbb{R}^{n_i \times n_i}$ is the inverse estimation error covariance $\boldsymbol{P}_i[k]$ of the Kalman filter. With these definitions, the prediction step of the DDIF can be stated as

$$\hat{\boldsymbol{y}}_i^-[k] = \boldsymbol{L}_i[k]\hat{\boldsymbol{y}}_i^+[k-1] + \boldsymbol{Y}_i^-[k]\boldsymbol{G}_i\boldsymbol{u}_i[k-1], \quad (19)$$
$$\boldsymbol{Y}_i^+[k] = \left[\boldsymbol{F}_i(\boldsymbol{Y}_i^+[k-1])^{-1}\boldsymbol{F}_i^{\mathrm{T}} + \boldsymbol{Q}_i\right]^{-1},$$

where $\hat{\boldsymbol{y}}_i^+[k]$ is the local *a priori* information state estimate at the current time step k and $\hat{\boldsymbol{y}}_i^+[k]$ the *a posteriori* one of the previous time step $k-1$. Parallel to the information state estimate, the corresponding *a posteriori* information matrix $\boldsymbol{Y}_i^+[k-1]$ is propagated forward to obtain the *a priori* information matrix $\boldsymbol{Y}_i^-[k]$. The local system noise covariance $\boldsymbol{Q}_i$ is derived from the global matrix $\boldsymbol{Q}$ as $\boldsymbol{Q}_i = \boldsymbol{T}_i\boldsymbol{Q}\boldsymbol{T}_i^{\mathrm{T}}$ and

$$\boldsymbol{L}_i = \boldsymbol{Y}_i^-[k]\boldsymbol{F}_i(\boldsymbol{Y}_i^+[k-1])^{-1}. \quad (20)$$

In the DDIF algorithm, as in the Kalman filter, the prediction step is followed by a measurement update or estimation step where the information state vector obtained by forward simulation is corrected using sensor data. Measurement signals $\boldsymbol{z}[k]$ are transformed to information space according to

$$\boldsymbol{i}[k] \coloneqq \boldsymbol{C}^{\mathrm{T}}\boldsymbol{R}^{-1}\boldsymbol{z}[k], \quad \boldsymbol{I} \coloneqq \boldsymbol{C}^{\mathrm{T}}\boldsymbol{R}^{-1}\boldsymbol{C}, \quad (21)$$

where $\boldsymbol{i}[k]$is defined as the *information state contribution* of the measurements $\boldsymbol{z}[k]$ and $\boldsymbol{I}[k]$ as its associated information matrix. Transformation to information state space is performed using the inverse measurement noise covariance $\boldsymbol{R}$ and the state space output mapping $\boldsymbol{C}$**.** The DDIF formulation allows for simple integration of information on the system received from other observer nodes into the current estimation step. Given the information state contribution $\boldsymbol{i}_j[k]$ of other nodes j, the estimation step is carried our as follows

$$\hat{\boldsymbol{y}}_i^+[k] = \hat{\boldsymbol{y}}_i^-[k] + \textstyle\sum_{j=1}^{N}\boldsymbol{T}_{ij}\boldsymbol{i}_j[k], \quad (22)$$
$$\boldsymbol{Y}_i^+[k] = \boldsymbol{Y}_i^-[k] + \textstyle\sum_{j=1}^{N}\boldsymbol{I}_{ij}.$$

Here, the matrices $\boldsymbol{T}_{ij}$ and $\boldsymbol{I}_{ij}$ express the transformation from the information state space of node j to the information state space of node $i$via the global state space. Therefore, it is important, that each local model is derived from the same global system. In principle, information of any number N of observer nodes can be incorporated into the current estimate. Arbitrary network topologies can be realized with the DDIF. In this contribution, ideal communication of information is assumed. Given the transformation (17) for an observer node j, the internodal transformations are

$$\boldsymbol{I}_{ij} = \left[\boldsymbol{T}_i\left[\boldsymbol{T}_i^{\mathrm{T}}\boldsymbol{I}_j\boldsymbol{T}_i\right]^{+}\boldsymbol{T}_i^{\mathrm{T}}\right]^{+}, \ \boldsymbol{T}_{ij} = \boldsymbol{I}_{ij}\boldsymbol{T}_i\boldsymbol{T}_j^{+}\boldsymbol{I}_j^{+}. \quad (23)$$

with an increasing number of observer nodes exchanging information with each other, estimation accuracy rises. However, so does the computational load and the amount of communicated data. In practice, a good balance needs to be found in accordance with requirements on accuracy, redundancy and fail-safe operation.

B. Decentralized Control

For control of the substructures, a decentralized optimal controller by means of an LQR control is designed for each subsystem i. The control laws for the input signals yield

$$\boldsymbol{u}_i[k] = \boldsymbol{K}_{\mathrm{lqr},i}\left(\hat{\boldsymbol{x}}_i^+[k] - \boldsymbol{x}_{\mathrm{d},i}[k]\right), \quad (24)$$

with the desired and estimated state $\boldsymbol{x}_{\mathrm{d},i}$ and $\hat{\boldsymbol{x}}_i^+[k]$. The feedback matrix $\boldsymbol{K}_{\mathrm{lqr},i} \in \mathbb{R}^{m_i \times n_i}$ is determined via the matrix Riccati equation with the cost function

$$J_i = \sum_{k=0}^{\infty}(\hat{\boldsymbol{x}}_i^+[k])^{\mathrm{T}}\boldsymbol{Q}_{\mathrm{lqr},i}\hat{\boldsymbol{x}}_i^+[k] + (\boldsymbol{u}_i[k])^{\mathrm{T}}\boldsymbol{R}_{\mathrm{lqr},i}\boldsymbol{u}_i[k]. \quad (25)$$

The weighting matrices $\boldsymbol{Q}_{\mathrm{lqr},i}$ and $\boldsymbol{R}_{\mathrm{lqr},i}$ are design parameters.

V. Results

In general, arbitrary connections between the distributed observers in Sec. IV-A are possible. In this contribution, we restrict the possible network topologies to three variants that are considered plausible for high-rise structures in practice. One in which there is no communication at all between local units, one where a module only communicates with its direct neighbors and one where observers are fully connected. The dynamic behavior of the structure depicted in Fig. 1 is simulated according to (6) with $\boldsymbol{\eta}_{\mathrm{p}} = 186$ primary eigenmodes. For those eigenmodes, the eigenfrequencies are below the Nyquist frequency when sampling the model at 1 kHz. The damping coefficients are set to $\alpha_1 = 0.05$ and $\alpha_2 = 0.005$. Gaussian noise is superimposed on the output $\boldsymbol{y}$ with a variance of $1.0 \times 10^{-8}\mathrm{m}^2$ for the strain measurements and $4.0 \times 10^{-6}\mathrm{m}^2$ for the camera-tracked displacements. The full camera output is allocated to all observers while each local module only accesses the strain measurements of sensors it contains. As a test scenario, we consider an initial deformation of the structure in the x-direction as caused e.g. by strong wind.

To compare the performance of the decentralized controllers for each variant, centralized LQG control is used as a reference. The central observer estimates the global state given the dynamic model (6) with $\boldsymbol{\eta}_{\mathrm{p}} = 10$ lowest magnitude primary eigenmodes. It is realized as an information filter according to Sec. IV-A, runs at a sampling frequency of 100 Hz and receives all available measurements. Noise is assumed to be uncorrelated

between states and sensor signals such that $\boldsymbol{Q}$ and $\boldsymbol{R}_i$ can be chosen as diagonal matrices.

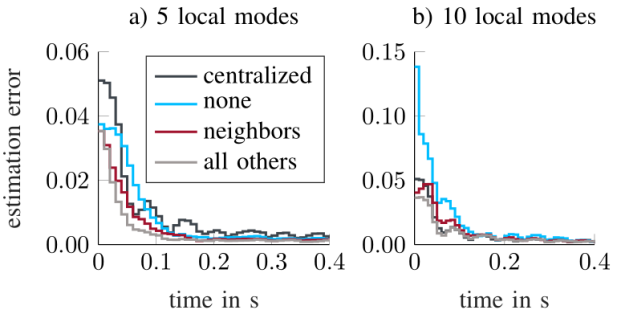

Fig. 2. Estimation error of the different observer realizations with respect to time

Each entry of $\boldsymbol{R}_i$ concerning a camera signal is set to $r_{\text{cam}} = 1.0 \times 10^{-6}\text{m}^2$, a value of $r_{\text{str}} = 1.0 \times 10^{-9}\text{m}^2$ is used for strain measurement covariance and all diagonal entries of $\boldsymbol{Q}$ are set to $q = 1.0 \times 10^{-2}$. For the corresponding centralized LQR, the state weight is chosen as $\boldsymbol{Q}_{\text{lqr},i} = 1.0 \times 10^{7} \cdot I$. Different control input weights are assigned to the actuators in each module as higher forces are required in lower modules to achieve comparable deformations. A control input weight factor of 1.0 is used for the first module, 4.0 for the second and 8.0 for the third where $\boldsymbol{R}_{\text{lqr},i}$ is again diagonal. The decentralized observers and controllers use the same set of parameters as their centralized counterparts. Regarding the local dynamic models, $\boldsymbol{\eta}_{\text{r}} = 10$ primary eigenmodes are used in the SEREP transformation (11) and $n_i = 5$ subsystem eigenmodes are retained in (15).

A comparison of observer performance in terms of the average estimation error over time is shown in Fig. 2. At each time step k, the estimation error is calculated according to

$$\tilde{\boldsymbol{x}}_i[k] = \sqrt{\frac{1}{2N_i}\sum_{l=1}^{2N_i}(x_i^l[k] - \hat{x}_i^l[k])^2} \tag{26}$$

where N_i is the number of DOFs an observer estimates, $\boldsymbol{x}_i[k] = [\boldsymbol{q}_i[k] \quad \dot{\boldsymbol{q}}_i[k]]^{\text{T}}$ the global or local state vector containing the DOFs and their derivatives with respect to time and $\hat{\boldsymbol{x}}_i[k]$ the corresponding state estimate. For decentralized observers, the estimation error is averaged over the four modules. We observe, that the centralized estimator has the highest estimation error of all observer realizations in Fig. 2 a) but converges faster than the decentralized observers without communication. This is surprising at first, but can be attributed to the smaller dimension of the local state spaces.

When choosing $n_i = 10$ primary subsystem eigenmodes for each local observer, i.e. the same number as for the centralized one, we obtain the result depicted in Fig. 2 b). Here, the performance of the centralized observer is superior to both the unconnected local estimators and the observers communicating with their neighboring units. Only in the fully connected topology, errors are comparable. For both $n_i = 5$ and $n_i = 10$ local subsystem eigenmodes, observer performance improves gradually with increased connectivity.

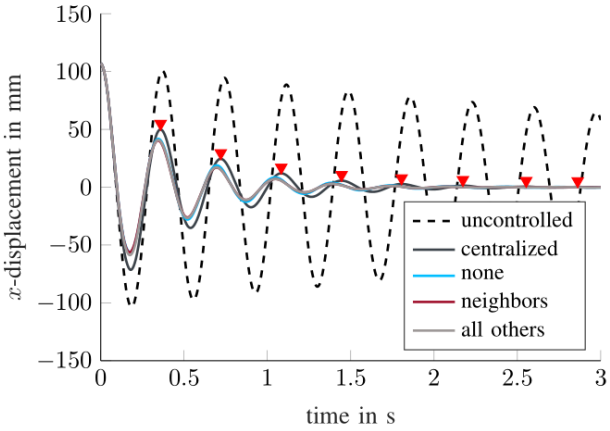

Fig. 3. Centralized and decentralized control response shown for the x-displacement of node 47.

Due to the low number of modules, going from interconnected neighbors to a fully connected topology results only in minor improvements. For the subsequent examination of controller performance, we use $n_i = 5$ local subsystem eigenmodes.

In Fig. 3, observer performance for both centralized control and the different variants of networked decentralized control is illustrated in a qualitative manner. The x-displacement of the node highlighted in pink in Fig. 1 is shown for the controlled cases and the uncontrolled one. In all scenarios with enabled controllers, the structural vibrations are damped almost completely within $t = 3$ s. The decentralized control responses are hardly discernible from each other. However, the damping is noticeably higher when comparing to the centralized LQR's response and a slight phase shift is visible. In order to further analyze the difference between control approaches, we define two performance measures. First, we consider the energy consumption of the actuators. It is obtained by multiplying the actuator forces with the corresponding element strain velocities and taking the absolute value. Summing up the result, we get the instantaneous total power demand which is integrated over all time steps to obtain the energy consumed over the simulation period of 3 s.

The second performance measure concerns the damping speed. As indicated in Fig. 3, the oscillation peaks of the control response are identified for the x-displacement of each node of the uppermost three stories. Fitting a function of the form

$$f(t) = a \cdot e^{bt} \tag{27}$$

to the obtained peak locations, the value of b can be used to quantify damping speed. A higher magnitude indicates stronger damping. The average coefficient $\bar{b}$ over all nodes considered is defined as the controller performance here.

In the following, both criteria are examined when using different parameters for the decentralized

controllers. The measures resulting for the centralized LQG controller using the parameters given above are used as a reference.

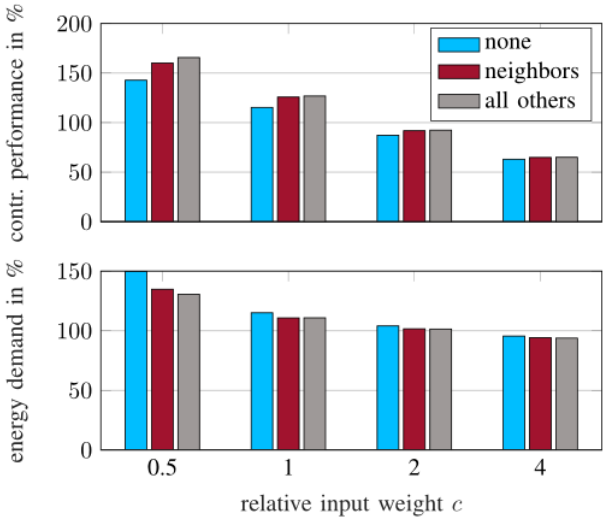

Fig. 4. Comparison of control performance and energy demand of decentralized controllers for different control input weights.

The most significant parameters for balancing energy demand and control performance are the LQR weights. In the following only $\boldsymbol{R}_{\mathrm{lqr},i}$ of the decentralized controllers is manipulated by multiplying it with a scale factor of $c = 0.5, 2$ and 4 respectively. The results are depicted in percent of the centralized reference measures in Fig. 4 for each scale factor. The decentralized control responses for a relative input weight of $c = 1$ that overlap in Fig 4, are discernible in terms of $\bar{b}$. There is no significant difference in both control performance and energy demand when all observers communicate and when only the neighbors exchange information. This also applies to $c = 2$ and $c = 4$. In the latter cases, we observe that approaching an energy demand comparable to the centralized reference comes with a considerable decrease in control performance. On the other hand, increased energy consumption for $c > 1$ yields significantly higher damping. Here, the difference between the network topologies becomes more pronounced. When spending about 20 % more energy as for $c = 1$, the fully connected modules achieve an increase in control performance of about 40 %. In the unconnected case, approximately the opposite is true. Given strong damping is desired, information exchange between local modules is crucial for good performance. In the range $c = 0.5 \ldots 2$ a good balance between the introduced performance criteria can be found according to their relative importance.

VI. Conclusion

With this contribution, we introduced a suitable approach for decentralized control of adaptive structures. Local subsystems are derived from a global FE model by means of model order reduction techniques. The SEREP-Guyan transformation combined with modal analysis yields local dynamic models of low order suitable for realizing decentralized control algorithms on low-cost hardware. Since the global dynamics can be reproduced locally using a transformation, the DDIF can be used for state estimation. This also enables the exchange of information between observer nodes by projecting back and forth between the local state spaces. We showed that performances comparable to centralized LQG control of the same structure can be achieved with the decentralized approach. By adjusting the parameters of local controllers, a suitable balance between their energy demand and damping response can be found that meets the design requirements. Increasing the interconnectedness of decentralized units can give a further performance boost. This depends, however, on the dimensions of the structure and the number of decentralized units and becomes more relevant in case of strong active damping. In further work, we want to consider structures of larger scale, where the networking aspect becomes more relevant.

Conflict of Interest

The authors declare no conflict of interest.

Author Contributions

Alexander Warsewa: Writing - original draft, Writing - review & editing, Methodology, Software, Visualization, Data curation; Julia L. Wagner**:** Writing - original draft, Writing - review & editing, Methodology; Michael Böhm: Conceptualization, Methodology, Writing - review & editing, Supervision; Oliver Sawodny: Supervision, Project administration, Funding acquisition; Cristina Tarín**:** Writing - review & editing, Supervision, Project administration, Funding acquisition; all authors had approved the final version.

References

[1] T. R. Naik, "Sustainability of concrete construction," *Practice Periodical on Structural Design and Construction*, vol. 13, no. 2, 2008.

[2] OECD, *Material Resources, Productivity and the Environment*, OECD Publishing Paris, 2015.

[3] W. Sobek and P. Teuffel, "Adaptive systems in architecture and structural engineering," *Smart Systems for Bridges, Structures, and Highways*, vol. 4330, 2001.

[4] N. Sandell, *et al*., "Survey of decentralized control methods for large scale systems," *IEEE Transactions on automatic Control*, vol. 23, no. 2, 1978.

[5] B. F. Spencer and S. Nagarajaiah, "State of the art of structural control," *Journal of Structural Engineering*, vol. 129, no. 7, 2003.

[6] D. D. Siljak, *Decentralized Control of Complex Systems*, Courier Corporation, 2011.

[7] Y. Lei, D. T. Wu, and Y. Lin, "A decentralized control algorithm for large-scale building structures," *Computer-Aided Civil and Infrastructure Engineering*, vol. 27, no. 1, 2012.

[8] F. R. Rofooei and S. Monajemi-Nezhad, "Decentralized control of tall buildings," *The Structural Design of Tall and Special Buildings*, vol. 15, no. 2, 2006.
[9] L. Bakule, B. Rehák, and M. Papík, "Decentralized networked control of building structures," *Computer-Aided Civil and Infrastructure Engineering*, vol. 31, no. 11, 2016.
[10] J. P. Lynch and K. H. Law, "Decentralized control techniques for large-scale civil structural systems," in *Proc. 20th Int. Modal Analysis Conference (IMAC XX)*, 2002.
[11] A. Warsewa, *et al*., "Decentralized and distributed observer design for large-scale structures using dynamic condensation," in *Proc. IEEE 15th International Conference on Automation Science and Engineering (CASE)*, 2019.
[12] A. G. O. Mutambara, *Decentralized Estimation and Control for Multisensor Systems*, CRC press, 1998.
[13] J. L. Wagner, et al., "On steady-state disturbance compensability for actuator placement in adaptive structures," *at-Automatisierungstechnik*, vol. 66, no. 8, 2018.
[14] F. Guerra, *et al*., "Deformation measurement of large buildings by holographical point replication," in *Optics for Arts, Architecture, and Archaeology VII*, vol. 11058, 2019.
[15] W. Gawronski, *Advanced structural dynamics and active control of structures*, Springer Science & Business Media, 2004.
[16] R. J. Guyan, "Reduction of stiffness and mass matrices," *AIAA Journal*, vol. 3, no. 2, 1965.
[17] J. O'Callahan and P. Li, "SEREP expansion," *Proceedings of the 14th International Modal Analysis Conference*, vol. 2768, 1996.
[18] P. Avitabile, "Model reduction and model expansion and their applications–part 1 theory," in *Proc. Twenty-Third International Modal Analysis Conference*, Orlando, FL, USA, 2005.
[19] D. Simon, *Optimal State Estimation: Kalman, H Infinity, and Nonlinear Approaches*, John Wiley & Sons, 2006.

Alexander Warsewa received the M. Eng. degree in mechanical engineering from the Toyohashi University of Technology, Japan, and the M.Sc. degree in medical engineering from the University of Stuttgart, Germany, in 2017. Since 2017, he is pursuing his Ph.D. at the Institute of System Dynamics, University of Stuttgart, Germany. His research interests include energy-based modeling of mechanical systems and state-space methods for distributed parameter systems.

Julia L. Wagner received the B.Sc. degree in medical engineering as a joint degree from the Universities of Stuttgart and Tübingen, Germany, in 2014. She finished her M.Sc. degree in the same course from the University of Stuttgart, Germany, in 2017. Since 2017, she is a research assistant and a Ph.D. candidate at the Institute for System Dynamics at the University of Stuttgart. Her research interests include analysis and control of adaptive structures.

Michael Böhm received the Dipl.-Ing. degree and Ph.D. in engineering cybernetics from the University of Stuttgart, Germany, in 2011 and 2017, respectively. Since 2017, he is the head of the construction systems engineering group at the Institute for System Dynamics. His current research interests include dynamic modeling and control of mechanical systems with applications to civil engineering.

Oliver Sawodny received the Dipl.-Ing. Degree in electrical engineering from the University of Karlsruhe, Karlsruhe, Germany, and the Ph.D. degree from the University of Ulm, Ulm, Germany, in 1991 and 1996, respectively. In 2002, he became a Full Professor with the Technical University of Ilmenau, Germany. Since 2005, he has been the Director of the Institute for System Dynamics at the University of Stuttgart, Germany. His research interests include methods of differential geometry, trajectory generation, and applications to mechatronic systems.

Cristina Tarín received the M.Sc. degree in electrical engineering from the Technical University of Valencia, Spain, in 1996, and the Ph.D. degree from the University of Ulm, Germany, in 2001. She has been teaching at the Universidad Carlos III of Madrid, Spain, and was enrolled in several research laboratories at the Technical University of Valencia, Spain. Since 2009, she has been a Full Professor with the Institute for System Dynamics, University of Stuttgart, Germany. Her main research interests are in signal processing and filtering, estimation and modeling.